Effect of Notch Geometry on the Plastic Behavior of Cu-Ag Composites

Rongmei Niu and Ke Han

***Abstract*—Understanding failure in conductive composites is critical for the design of reliable electrical components. Using strain mapping, we studied the effect of notch geometry on mechanical properties and the mechanisms of notch-related plastic deformation. Our study clearly revealed notch strengthening in Cu-Ag nanocomposites. In all notched samples, we found highly localized necking bands between pairs of notches. Under tension, these bands developed into ellipse loops. Within the bands, deformation strain was much higher than the average strain over a large neighboring area. The plasticity of necking bands depended on notch tip radii. In samples whose notch tip radius was $\sim$ 3.81 mm, the localized strain within necking bands reached as high as 50%. In samples with sharper notches ($\sim$0.20 mm), necking plasticity still attained 18% before failure. The results of this study provide unique insights into the endurance and performance of high-strength composites.**

***Index Terms*—Copper alloys, deformation, high-strength, notch geometry, stress concentration.**

I. Introduction

CU-BASED composites have numerous applications where an excellent combination of mechanical strength and electrical conductivity is required. The strength of Cu composites is enhanced through cold working [1], [2], grain refinement [3], [4], [5], and nano-particles dispersion strengthening [6], [7], [8], [9], [10]. Typical conductors for high field magnets are Cu-based metal-metal composites, such as Cu–Ag [11], [12], Cu–Nb [13], [14], [15], [16], and metal-ceramic matrix composites, such as Cu-Al_2O_3 [8], [17].

The fabrication of high-strength conductors requires high deformation strain to create high densities of dislocations or interfaces. Depending on its processing history, conductor material may contain significant structural defects such as voids, internal cracks (such as chevron), and second-phase particles. For instance, during handling, surface defects, such as deep scratches, grooves, or shear burrs, are often introduced. These defects can have a major adverse effect on the ductility and workability. Conductor materials that are sensitive to surface scratches (notch sensitivity) can develop major flaws and have poor bendability due to premature cracking.

Manuscript received 26 October 2023; revised 7 December 2023; accepted 25 December 2023. Date of publication 8 January 2024; date of current version 24 January 2024. This work was supported in part by the National Science Foundation under Grant DMR-1157490, in part by the State of Florida, and in part by the U.S. Department of Energy. *(Corresponding author: Ke Han.)*

The authors are with the National High Magnetic Field Laboratory, Tallahassee, FL 32309 USA (e-mail: han@magnet.fsu.edu).

Color versions of one or more figures in this article are available at https://doi.org/10.1109/TASC.2024.3350589.

Digital Object Identifier 10.1109/TASC.2024.3350589

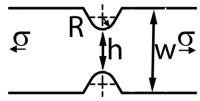

Fig. 1. V-notch geometry: w = 6 mm in Cu-Ag wire. Strength is calculated using h.

For these materials to be reliable, it is critical to understand the effects of notches, flaws, and geometric discontinuities on their mechanical properties. Ductility measurements on standard smooth tensile specimens do not always reveal metallurgical or environmental changes that lead to reduced local ductility. The tendency for reduced ductility in the presence of a triaxial stress field and steep stress gradients (such as occurring at a notch) is called notch sensitivity [18]. In high-strength nanocomposites, where metals exhibit very limited elongation because of small distance between strengthening particles and scarcity of dislocations in nanoscale lamellae structure [19], [20], [21], [22], notch sensitivity may be expected to be different from their coarse-grained counterparts [23], [24], [25], [26].

A common way of evaluating notch sensitivity is tension tests using notched specimens [18]. The purpose of this work is to provide insight into the effects of notches on mechanical properties and local plasticity in high-strength conductors.

II. Experimental Methods

A. Materials and Fabrication

In this investigation, we used rectangular Cu25wt%Ag wires (4 x 6 mm^2) cold-drawn by MagLab [27]. All materials were measured using x-y-z coordinates, with x indicating the longitudinal direction of drawing, y indicating the transverse direction (width), and z indicating the short-transverse direction (thickness). The tension axis was longitudinal, i.e., parallel to the x-axis.

To examine the mechanics of constrained yielding, we cut deliberately matching pairs of V-shaped notches perpendicular to the loading axis in the width direction. We planned for the cross-section area of a sample between notch pair tips to be one-half of the remaining area of the sample lying outside of the notches but within the gauge length of 20 mm. The notch angle was held constant at 60 degrees. The notch tip radius (NTR) ranged from 0.20 mm to 3.83 mm, as measured using the video system iNEXIV VMA-2520, see Table I. For a representative image of a double-notched tensile specimen, see Fig. 1.

TABLE I
NOTCH SIZE-DEPENDENT MECHANICAL PROPERTIES IN CUAG WIRES

Notch tip radius, mm	σ_N OR UTS (MPa)	NSR (GPa)	Elongation (%)	
			NT	LA
0.20	1165	1.18	18.5	2.53
0.25	1167	1.18	23	3.3
0.51	1135	1.15	27.3	2.7
1.02	1108	1.12	31.2	2.9
1.28	1093	1.10	42.5	4.3
2.55	1052	1.06	35.5	6.8
3.83	1028	1.04	50	5.9

σ_N represents notch strength for notched samples and UTS for smooth samples.
Notch tip radius was measured values.
NSR: notch strength ratio.
Elongation was measured from a rectangular area of 0.1 mm x 0.1 mm at the notch tip (NT), 15 mm x 8.4 mm large area (LA) around notches.

B. Deformation Strain Examination

For overall plasticity evaluation, an extensometer or strain gauge has been used for measuring strain. However, for local deformation measurement, the regular method for measuring strain was not applicable because of the long coverage of the extensometer, and it would not discriminate between areas with significant deformation and those without. A Digital Image Correlation (DIC) system was employed to monitor the strain at the notch tip (NT) vicinity. We measured an average strain in an area of 0.1×0.1 mm^2 at the NT (see Fig. 2(a)), compared with conventional strain measurement over a large area. The elongation measured in this work is referred to as the strain to initiate cracks not to fracture. Since, in this study, the strain was measured locally by DIC at the NT and was not averaged to undeformed areas, it reflected the real plasticity in that area.

C. Mechanical Tests

Tensile tests were carried out on both notched and smooth (un-notched) samples on a MTS machine with a load cell of 20KN. The strain rate is 0.5mm/min. Notch strength (σ_N) was defined as the maximum load divided by the net cross-sectional area (h multiplied by thickness in Fig. 1) at the notch.

III. RESULTS AND DISCUSSIONS

A. Notch Effect in CuAg Wires

A common way to characterize notch sensitivity is to determine the Notch Strength Ratio (NSR) [18], [28]. NSR is calculated by $= \sigma_N$/UTS, where UTS is the ultimate tensile strength of a smooth sample, and σ_N is the notch strength, i.e., the nominal UTS of the notched sample. The UTS of our Cu-Ag wires without notches was 903 ± 1 MPa [27]. The NSR values were all above 1 in samples whose notch tips had radii between 0.2 mm and 3.8 mm. The introduction of notches increased σ_N, indicating a "notch strengthening" effect (NSR > 1). It reached its maximum value of 1167 MPa at a NTR of 0.20 mm, an increase of 18% over the UTS of smooth samples. The values for notch strength and notch radius appeared to follow a linear relationship: σ_N = -38NTR+1160, (0.2mm$\leq$R$\leq$3.8mm).

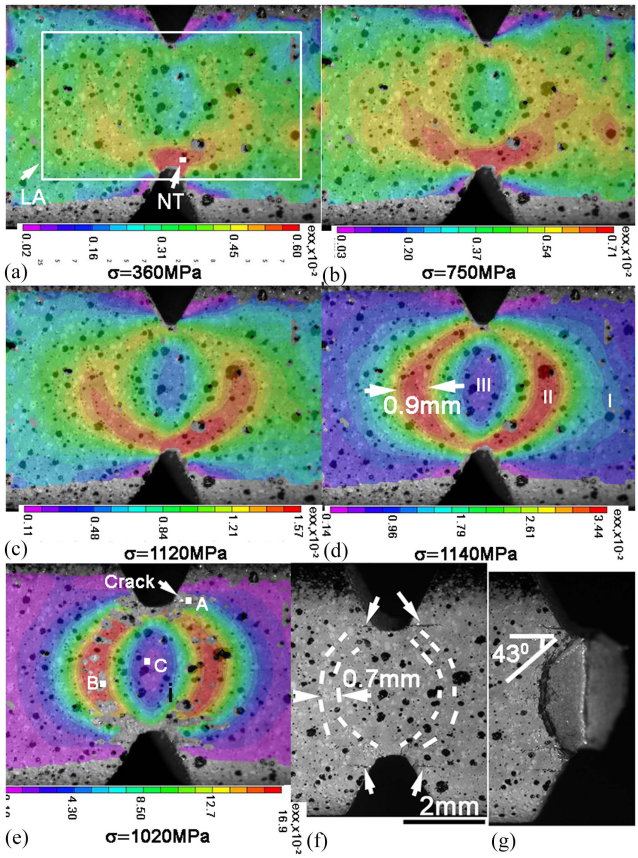

Fig. 2. e_{xx} distribution across the CuAg sample surface at the notch tip (R=0.20mm) under various levels of tensile stress. The horizontal color bar represents local strains. (a) e_{xx} of 360 MPa: non-uniform strain distribution at early loading. Average strain value in Large Area (LA) is measured within the rectangle enclosed by white lines. NT indicates location of Notch Tip for quantitative strain measurement. (b) e_{xx} of 750 MPa: Areas with higher e_{xx} are scattered in the vicinity of the notch. (c) e_{xx} of 1120 MPa: deformation starts localizing; by this time, the notch has widened by ~3.8%. (d) e_{xx} of 1140 MPa: necking bands develop in Zone II. By comparison, Zones I and III are less deformed. The inner radius of Zone II is $\sim 1.8 \pm 0.5$mm. The notch has widened by ~9.3%. (e) e_{xx} of 1020 MPa: the inner radius of Zone II is $\sim 2.0 \pm 0.6$mm. The notch has widened by ~37.5%. The plastic deformation has blunted the notch tips. Long cracks parallel to the loading direction appear at the transition from Zone I to Zone II. (f) An in-situ capture of the notched sample under tension before fracture, exhibiting microcracks developing and propagating within the necking bands in Zone II. The sharp notches have become blunted and stretched. (Necking width was estimated along the white dash lines that mark the boundary of the necking band area). (g) A fracture appearing across the necking band and slipping off along the shear direction.

Average elongation was first measured in a 15 mm long x 8.4 mm wide area of each sample, defined as the Large Area (LA). In CuAg wire with opposite notch pairs, average elongation was less than in wires without any notches. The sharper the notches, the less the average elongation (Table I). The average elongation of smooth CuAg wire was 5-8% [20]. It decreased to 4.3% with the NTR reducing to 1.28mm. When the NTR was reduced to 0.52mm, the LA elongation was reduced by 50%.

The Notch Tip (NT) was subjected to higher strain than its surroundings. The elongation at NT in our samples was therefore higher than the LA elongation. For example, the NT elongation in the Cu-Ag sample was 50% at 3.83mm NTR, while The LA elongation was as low as 5-8%. At a sharp NTR of 0.52 mm, NT

elongation was still as high as 27%. At an even sharper NTR of 0.20 mm, NT elongation was reduced significantly but still was about 18%. CuAg sheets with similar strength showed similar high local plasticity. In these sheets, elongation were as high as 30% [21] in slip bands.

50% elongation deformation in CuAg was equivalent to a true strain of 0.41, which was less than the true strain values 0.66 and 0.88 that were measured by fractured cross-section areas in our earlier CuAg wire work [20]. The true strain accumulated during deformation from the initial ingot to the final wire was ~4. Taken together, the true strain accumulated at NT was about 4.41, which was still below 5.8, the reported maximum drawing true strain in CuAg without breakage [29]. In other words, our measurement of 50% plastic deformation at the NT seems justified.

B. Tension Strain Along the Loading Axis

To study the impact of notches on the deformation mechanism, we selected the samples with the sharpest notches (NTR of 0.2 mm) and thus the most notch constraint on strain. When tension was applied to these samples, strain distribution was not uniform across the whole area, even during the elastic stage. Higher tensile strain (e_{xx}) appeared in the vicinity of the NT. When tensile stress (σ) reached 360 MPa, tensile strain (e_{xx}) reached 0.31% at NT. At the segment center between the notch pair, the strain level was 0.14%, approximately half that of the NT. On the same sample, the strain level for the LA was 0.17%, slightly more than half that of the NT. The LA in this case was a 15.0 x 8.4 mm^2 rectangle (see Fig. 2(a)). As expected, the presence of notches resulted in non-uniform deformation.

As loading stress approached the proportional limit of NT (~750 MPa), NT strain increased to 0.7% while LA strain remained at 0.4% (see Fig. 2(b)). As loading stress approached the proportional limit of the notch center (~1120 MPa), NT strain increased rapidly, reaching as high as 1.5% while LA strain remained at 0.18% (Fig. 3(a)). Meanwhile, a set of two narrow bands, originating at the NTs, became visible. The inclination angles with respect to the tensile direction of both bands were each between 35° and 40° at the onset of localized necking. Within the bands, the material was highly strained. Further loading aggravated this localized deformation (from now on referred to as necking bands). The two necking bands came together and developed into an elliptical necking loop (see Fig. 2(d)) when the notch stress reached its maximum value of 1165 MPa. The inner radius of this necking loop was about 1.8 ± 0.5 mm at 1140 MPa. Using this necking loop, we defined three deformation zones: Zone I, far away from the notched area and outside of the elliptical necking loop; Zone II, the most deformed area (also called the zone of necking bands), characterized by a dense strain-gradient distribution; Zone III, the center of the segment between notches.

After yielding, as necking proceeded, NTs appeared significantly blunt. The notch radius increased by 55% at 1140 MPa (see Fig. 2(d)) and the notch bottom became flattened. The blunting of the NT indicated great plastic deformation in this area. Meanwhile, microcracks became visible in Zone II. From

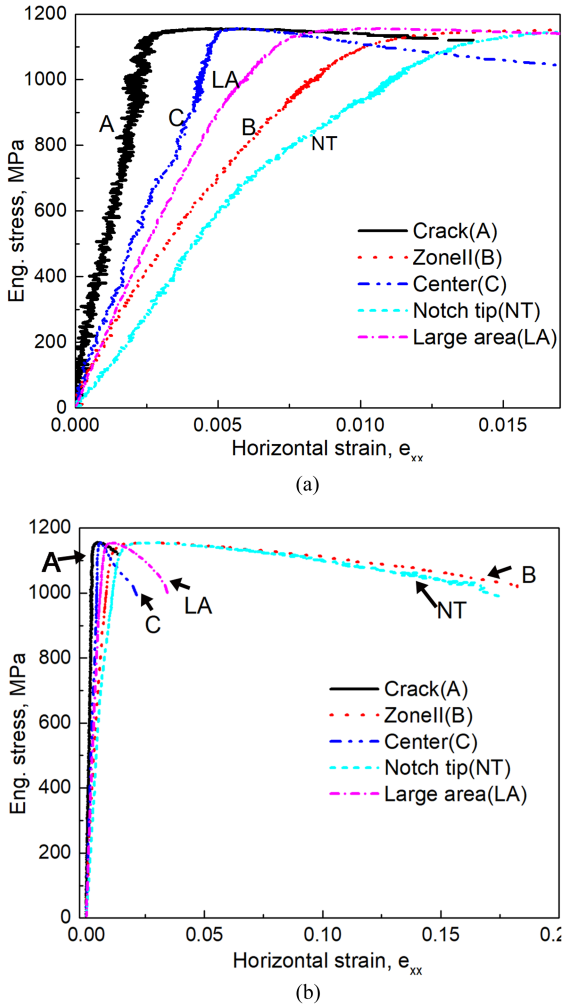

Fig. 3. Stress vs. local strain e_{xx} in CuAg samples with NTR of 0.20mm. (a) In earlier strain stage; (b) till fracture. ["Crack", "Zone II" and "Center" represent the strains from sites A, B, and C in Fig. 1(e). "Large Area" and "Notch Tip" were marked in Fig. 2(a)].

the location of these microcracks, we estimated the necking width (see Fig. 2(f)). The necking width was about 0.7-0.8 mm on each side of the notch segment. This was very close to the 0.9 mm measured by DIC-strain mapping when stress reached almost to its highest level. In our sample, final failure started in Zone II (see Fig. 2(g)). The inclination angle of the fractured surface at the NT, with respect to the tensile axis, was ~43°. At the NT, the fracture angle was slightly different from the initial deformation-band angle.

To quantify the strain difference for each zone, we analyzed the strain in three representative Sites, A, B, and C. We also compared the strain at the NT to the average strain of the LA. Site A was located at a horizontal crack next to the notch. Site B was in the center of Zone II, well away from the notch. Site C was at the segment center between the pair of notches. Each of these sites measured 0.1x0.1mm^2. Location-dependent deformation behavior was very different (see Fig. 3).

Both Sites A and C had short elastic stages. Site B and the NT area had relatively long elastic stages, see Fig. 3. During the elastic stages, the slopes of stress-strain curves at Sites A,

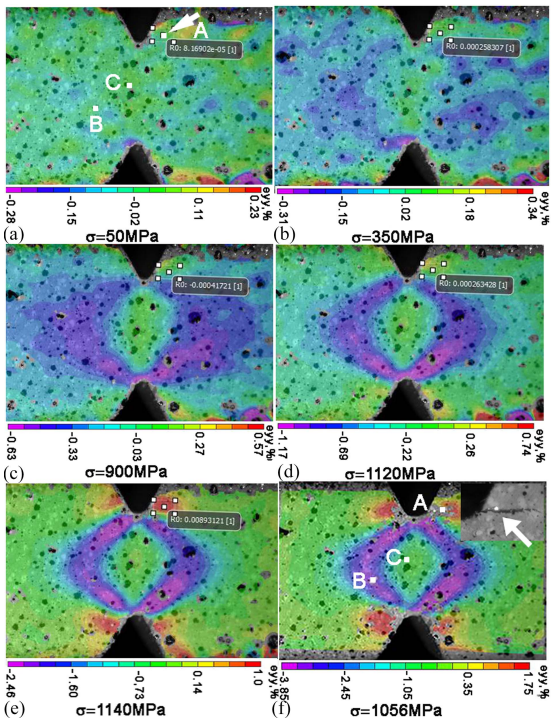

Fig. 4. e_{yy} distribution in a CuAg wire around the upper and lower notches (R=0.20mm). (a) The e_{yy} distribution in the earlier elastic stage (σ=50 MPa). The larger white squares marked "A," "B," and "C" indicate the three locations where e_{yy} strain monitoring was performed. (Site "A" was selected because the crack originated there; Site "B" was selected because it was in Zone II at later loading; Site "C" was selected to represent the center of the notch section). (b) The e_{yy} distribution at σ=350 MPa. At this load, negative strain ($-e_{yy}$) begins to appear in selected locations. Site "B" is under contraction while Sites "A" and "C" are slightly tensioned. (c) The e_{yy} distribution at σ=900 MPa. (d) The e_{yy} distribution at σ=1120 MPa. Negative strain ($-e_{yy}$) localization begins to concentrate in a region corresponding to Zone II in Fig. 2. Contraction strain at "B" increases more rapidly than at "A" or "C". (e) The e_{yy} distribution at σ=1140 MPa. High e_{yy} strain begins to appear in site A. (f) The e_{yy} distribution at σ=1056 MPa. In the ellipse zone (zone II), maximum contraction strain occurs. At Site "A," cracking appears because e_{yy} increases rapidly to its maximum tensile strain once yielding has occurred. This cracking then relieves stress by 84 MPa (from 1140 to 1056 MPa).

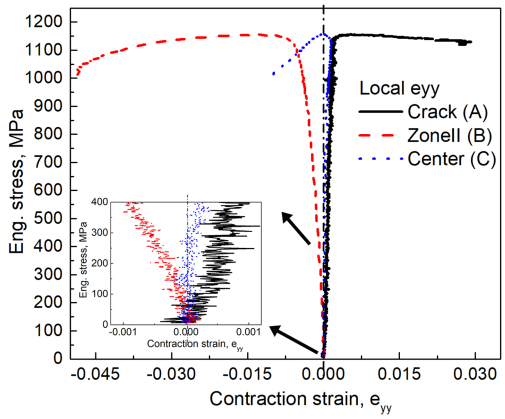

Fig. 5. Loading stress vs. local strain (e_{yy}) curves in a CuAg sample with NTR of 0.2 mm. The three curves represent strain values at three locations [A, B, and C in Fig. 4(f)]: the crack site (solid line), Zone II (dashed line), and the notch segment center (dash-dot line). The inset shows the stress-strain curves at low stress levels.

C, LA, B, and NT were 397 ± 14 GPa, 212 ± 3 GPa, 178 ± 6 GPa, 132 ± 5 GPa, and 124 ± 1 GPa, respectively. The slope difference reflected the stress concentration condition around the notches. In high-stress locations, the slope was low; in low-stress locations, the slope was high. Materials yielded more quickly in high-stress locations. In the NT and at Site B, for example, the materials not only yielded and plastically deformed much earlier than in other regions, but also had approximately the same total deformation strain before failure (16.6% at the NT, 17.7% at Site B, see Fig. 3(b)). Sites A and C were barely deformed: the maximum e_{xx} strain values in those areas were only 1.6% and 1.0%, respectively. Plastic strain values at NT and Site B were about sixteen times higher than at Site C.

C. Contraction Perpendicular to Loading Direction (e_{yy} Strain)

It is common for cracking to be perpendicular to the loading direction, but we noticed that long cracks also developed parallel to the loading direction (see Fig. 2(e) and (f)). Because of that, we investigated the e_{yy} strain evolution. These long cracks were located between Zone I and Zone II, which was a much less stressed area, where the e_{xx} strain was only 1.4%.

According to the Poisson effect, materials contract in directions perpendicular to the loading direction. To investigate notch-related e_{yy} distribution, we analyzed three representative locations: Site A, at the crack locations; Site B, in zone II; and Site C in the notch segment center (Cf Figs. 2 and 4). We plotted the curves of engineering (Eng.) stress vs. e_{yy} strain at these three points (Fig. 5). Values for Eng. stress was a ratio of the applying load to the original net notch cross-section area.

In the early elastic stage ($\sigma \leq$100 MPa), all zones were at almost the same strain level. In this stage, e_{yy} distribution was uniform throughout our sample (e.g., Sites A, B, and C in Figs. 4(a) and 5). This was no longer true, however, once loading stress reached between 100 and 350 MPa. By this stage, e_{yy} distribution was clearly no longer uniform, and areas with negative e_{yy} (contraction strain) had developed in various locations (Figs. 4(b) and 5). Subsequently, these scattered areas grew and merged, forming a localized negative e_{yy} zone. This localized contraction occurred in Zone II (Fig. 2). The contraction strain increased rapidly at Site B, which experienced more contraction than other regions. By contrast, both Site A and Site C had positive e_{yy}. At these sites, samples were only slightly stretched within the elastic stage. The slopes of engineering stress vs. local strain at Site A, Site B, and Site C in Fig. 5 were 512GPa, -215GPa, and 730 GPa, respectively.

With further loading,$\sigma \geq$1140 MPa, the tension plastic deformation at Site A became pronounced, see Figs. 4(e) and 5. A crack appeared at Site A when the strain reached ∼2.7%, Meanwhile, a contraction strain at Site B increased significantly to 4.6%. Strain at Site C switched from tension to contraction along with the development of highly contracted strain in Zone II. The maximum contraction strain was ∼ 1.2% at Site C.

Horizontal cracks were found in our samples only when the NT radii were small ($\leq$ 0.52 mm). At the notch radius of 1.02mm

and 2.55mm, the maximum e_{yy} strain at Site A reduced to 2.2% and 0.1%, respectively (see Fig. 4(b)). When the notch radius increased to 3.83 mm, e_{yy} strain at Site A switched from tension to contraction. Away from the notch area, measured contraction strain reached as high as 8.2%, effectively preventing the development of horizontal cracks in any of the samples in which Site A was under contraction.

IV. Conclusion

Notched Cu-Ag nanocomposites, when compared with smooth counterparts, showed a unique tensile behavior. Notch strength, notch tip strain concentration, and deformation behavior were identified as functions of the notch tip radius. Cu-Ag nanocomposites under uniaxial tension had low notch sensitivity (i.e., notch strength ratio >1). Localized necking bands developed between notch pairs. The elongation of failure in the necking bands was proportional to the notch tip radius. Deformation was much lower outside of localized necking bands.

Acknowledgment

The authors thank William Starch for drawing and Mary Tyler for editing.

References

[1] J. B. Dubois, L. Thilly, F. Lecouturier, P. Olier, and P. O. Renault, "Cu/Nb nanocomposite wires processed by severe plastic deformation for applications in high pulsed magnets: Effects of the multi-scale microstructure on the mechanical properties," *IEEE Trans. Appl. Supercond.*, vol. 22, no. 3, Jun. 2012, Art. no. 6900104, doi: 10.1109/TASC.2011.2174574.

[2] J. D. Verhoeven et al., "Development of deformation processed copper-refractory metal composite alloys," *J. Mater. Eng.*, vol. 12, no. 2, pp. 127–139, Jun. 1990, doi: 10.1007/BF02834066.

[3] K. Han ¶, R. P. Walsh, A. Ishmaku, V. Toplosky, L. Brandao, and J. D. Embury, "High strength and high electrical conductivity bulk Cu," *Philos. Mag.*, vol. 84, no. 34, pp. 3705–3716, Dec. 2004, doi: 10.1080/14786430412331293496.

[4] R. Niu and K. Han, "Strain hardening and softening in nanotwinned Cu," *Scripta Materialia*, vol. 68, no. 12, pp. 960–963, Jun. 2013, doi: 10.1016/j.scriptamat.2013.02.051.

[5] R. Niu, K. Han, Y.-.. Su, T. Besara, T. M. Siegrist, and X. Zuo, "Influence of grain boundary characteristics on thermal stability in nanotwinned copper," *Sci. Rep.*, vol. 6, no. 1, Aug. 2016, Art. no. 31410, doi: 10.1038/srep31410.

[6] A. Morozova, R. Mishnev, A. Belyakov, and R. Kaibyshev, "Microstructure and properties of fine grained Cu-Cr-Zr alloys after termo-mechanical treatments," *Rev. Adv. Mater. Sci.*, vol. 54, no. 1, pp. 56–92, 2018, doi: 10.1515/rams-2018-0020.

[7] B. An, Y. Xin, R. Niu, J. Lu, E. Wang, and K. Han, "Hardening Cu-Ag composite by doping with Sc," *Mater. Lett.*, vol. 252, pp. 207–210, Oct. 2019, doi: 10.1016/j.matlet.2019.05.101.

[8] K. Han, R. E. Goddard, V. Toplosky, R. Niu, J. Lu, and R. Walsh, "Alumina particle reinforced Cu matrix conductors," *IEEE Trans. Appl. Supercond.*, vol. 28, no. 3, 2018, Art. no. 7000305, doi: 10.1109/TASC.2018.2795587.

[9] R. Niu, V. J. Toplosky, J. W. Levitan, J. Lu, and K. Han, "Deformation induced precipitation in CuCrZr composites," *Mater. Sci. Eng.: A*, vol. 875, Jun. 2023, Art. no. 145092, doi: 10.1016/j.msea.2023.145092.

[10] R. Niu, V. Toplosky, and K. Han, "Cryogenic temperature properties and secondary phase characterization of CuCrZr composites," *IEEE Trans. Appl. Supercond.*, vol. 32, no. 6, 2022, Art. no. 4300405, doi: 10.1109/TASC.2022.3152992.

[11] Y. Sakai, K. Inoue, and H. Maeda, "New high-strength, high-conductivity Cu-Ag alloy sheets," *Acta Metallurgica et Materialia*, vol. 43, no. 4, pp. 1517–1522, Apr. 1995, doi: 10.1016/0956-7151(94)00376-S.

[12] C. Zhao et al., "Improvement of properties in Cu–Ag composites by doping induced microstructural refinement," *Mater. Sci. Eng.: A*, vol. 799, Jan. 2021, Art. no. 140091, doi: 10.1016/j.msea.2020.140091.

[13] W. A. Spitzig and P. D. Krotz, "Comparison of the strengths and microstructures of Cu-20% Ta and Cu-20% Nb in situ composites," *Acta Metallurgica*, vol. 36, no. 7, pp. 1709–1715, Jul. 1988, doi: 10.1016/0001-6160(88)90238-6.

[14] L. Thilly, M. Véron, O. Ludwig, F. Lecouturier, J. P. Peyrade, and S. Askénazy, "High-strength materials: In-situ investigations of dislocation behaviour in Cu-Nb multifilamentary nanostructured composites," *Philos. Mag. A*, vol. 82, no. 5, pp. 925–942, Mar. 2002, doi: 10.1080/01418610208240010.

[15] J. D. Verhoeven et al., "The resistivity and microstructure of heavily drawn Cu-Nb alloys," *J. Appl. Phys.*, vol. 65, no. 3, pp. 1293–1301, 1989, doi: 10.1063/1.343024.

[16] L. Deng et al., "Response of microstructure to annealing in in situ Cu–Nb microcomposite," *J. Mater. Sci.*, vol. 54, no. 1, pp. 840–850, Jan. 2019, doi: 10.1007/s10853-018-2865-4.

[17] K. Han et al., "Properties of selected high-strength composite conductors with different strengthening components," *IEEE Trans. Appl. Supercond.*, vol. 30, no. 4, 2020, Art. no. 4301305, doi: 10.1109/TASC.2020.2981270.

[18] G. E. Dieter, "Mechanical behavior under tensile and compressive loads," *Mech. Testing Eval.: ASM Int.*, vol. 8, 2000, Art. no. 25425, doi: 10.31399/asm.hb.v08.a0003261.

[19] W. D. Nix, J. R. Greer, G. Feng, and E. T. Lilleodden, "Deformation at the nanometer and micrometer length scales: Effects of strain gradients and dislocation starvation," *Thin Solid Films*, vol. 515, no. 6, pp. 3152–3157, Feb. 2007, doi: 10.1016/j.tsf.2006.01.030.

[20] K. Han et al., "The fabrication, properties and microstructure of Cu–Ag and Cu–Nb composite conductors," *Mater. Sci. Eng.: A*, vol. 267, no. 1, pp. 99–114, Jul. 1999, doi: 10.1016/S0921-5093(99)00025-8.

[21] R. Niu and K. Han, "Pockets of strain-softening and strain-hardening in high-strength Cu-24wt%Ag sheets," *J. Mater. Sci.*, vol. 58, no. 21, pp. 8981–8989, Jun. 2023, doi: 10.1007/s10853-023-08519-y.

[22] R. Niu, K. Han, Z. Xiang, L. Qiao, and T. M. Siegrist, "Ultra-high local plasticity in high-strength nanocomposites," *J. Mater. Sci.*, vol. 55, no. 31, pp. 15183–15198, Nov. 2020, doi: 10.1007/s10853-020-05097-1.

[23] R. W. Karry and T. J. Dolan, "Influence of grain size on fatigue notch-sensitivity," *Amer. Soc. Testing Mater.*, vol. 53, pp. 789–804, 1953.

[24] P. Lorenzino and A. Navarro, "Grain size effects on notch sensitivity," *Int. J. Fatigue*, vol. 70, pp. 205–215, Jun. 2015, doi: 10.1016/j.ijfatigue.2014.09.012.

[25] K. Youssef, M. Sakaliyska, H. Bahmanpour, R. Scattergood, and C. Koch, "Effect of stacking fault energy on mechanical behavior of bulk nanocrystalline Cu and Cu alloys," *Acta Materialia*, vol. 59, no. 14, pp. 5758–5764, Aug. 2011, doi: 10.1016/j.actamat.2011.05.052.

[26] T. A. Furnish et al., "Fatigue stress concentration and notch sensitivity in nanocrystalline metals," *J. Mater. Res.*, vol. 31, no. 6, pp. 740–752, Mar. 2016, doi: 10.1557/jmr.2016.66.

[27] R. Niu, K. Han, Z. Xiang, L. Qiao, and T. M. Siegrist, "Ultra-high local plasticity in high-strength nanocomposites," *J. Mater. Sci.*, vol. 55, no. 31, pp. 15167–15182, Nov. 2020, doi: 10.1007/s10853-020-05076-6.

[28] R. T. Qu, M. Calin, J. Eckert, and Z. F. Zhang, "Metallic glasses: Notch-insensitive materials," *Scripta Materialia*, vol. 66, no. 10, pp. 733–736, May 2012, doi: 10.1016/j.scriptamat.2012.01.044.

[29] Y. Sakai and H. J. Schneider-Muntau, "Ultra-high strength, high conductivity Cu-Ag alloy wires," *Acta Materialia*, vol. 45, no. 3, pp. 1017–1023, Mar. 1997, doi: 10.1016/S1359-6454(96)00248-0.